Benzylic Oxidation of Gemfibrozil-1-*O*-*β*-Glucuronide by P450 2C8 Leads to Heme Alkylation and Irreversible Inhibition

Brian R. Baer,* Robert Kirk DeLisle, and Andrew Allen

Department of Drug Metabolism, Array Biopharma Inc., 3200 Walnut Street, Boulder, Colorado 80301

Received March 16, 2009

Gemfibrozil-1-*O*-*β*-glucuronide (GEM-1-*O*-gluc), a major metabolite of the antihyperlipidemic drug gemfibrozil, is a mechanism-based inhibitor of P450 2C8 in vitro, and this irreversible inactivation may lead to clinical drug−drug interactions between gemfibrozil and other P450 2C8 substrates. In light of this in vitro finding and the observation that the glucuronide conjugate does not contain any obvious structural alerts, the current study was conducted to determine the potential site of GEM-1-*O*-gluc bioactivation and the subsequent mechanism of P450 2C8 inhibition (i.e., modification of apoprotein or heme). LC/MS analysis of a reaction mixture containing recombinant P450 2C8 and GEM-1-*O*-gluc revealed that the substrate was covalently linked to the heme prosthetic heme group during catalysis. A combination of mass spectrometry and deuterium isotope effects revealed that a benzylic carbon on the 2′,5′-dimethylphenoxy group of GEM-1-*O*-gluc was covalently bound to the heme of P450 2C8. The regiospecificity of substrate addition to the heme group was not confirmed experimentally, but computational modeling experiments indicated that the *γ*-meso position was the most likely site of modification. The metabolite profile, which consisted of two benzyl alcohol metabolites and a 4′-hydroxy-GEM-1-*O*-gluc metabolite, indicated that oxidation of GEM-1-*O*-gluc was limited to the 2′,5′-dimethylphenoxy group. These results are consistent with an inactivation mechanism wherein GEM-1-*O*-gluc is oxidized to a benzyl radical intermediate, which evades oxygen rebound, and adds to the *γ*-meso position of heme. Mechanism-based inhibition of P450 2C8 can be rationalized by the formation of the GEM-1-*O*-gluc-heme adduct and the consequential restriction of additional substrate access to the catalytic iron center.

Introduction

Reports of clinical pharmacokinetic interactions between gemfibrozil (GEM)[1] and P450 2C8 substrates such as cerivastatin, repaglinide, rosiglitazone, and pioglitazone have prompted in vitro investigations into the mechanism of these drug−drug interactions (*1*−*4*). Initial in vitro experiments, performed in human liver microsomes, demonstrated that GEM was a moderate inhibitor of P450 2C9 (IC_{50} = 9.6 *μ*M) but a relatively weak inhibitor of P450 2C8 activity toward cerivastatin (IC_{50} = 95 *μ*M) (*5, 6*). Yet, in vivo, there were no drug−drug interactions observed with the P450 2C9 substrate, warfarin (*7*). Subsequent work by Shitara et al. revealed that the gemfibrozil-1-*O*-*β*-glucuronide metabolite (GEM-1-*O*-gluc) was a more potent inhibitor than GEM (IC_{50} values are 4.1 and 28 *μ*M, respectively) of recombinant P450 2C8 activity toward cerivastatin, therefore offering a possible explanation for the drug−drug interactions observed in vivo (*8*). This glucuronide metabolite is primarily formed by the human UDP-glucuronosyltransferase (UGT) 2B7 isozyme, as determined by the relative turnover in a panel of recombinant human UGT isozymes, and by correlation studies with UGT2B7-specific substrates in human liver microsomes (*9*).

Ogilvie et al. confirmed the competitive inhibition of P450 2C8 by GEM-1-*O*-gluc in human liver microsomes and, in addition, found that preincubation of the inhibitor further lowered the IC_{50} for inhibition of P450 2C8-mediated paclitaxel metabolism (IC_{50} = 24 to 1.8 *μ*M) (*10*). This time-dependent inhibition of P450 2C8 was not observed with the parent drug, GEM, and neither the substrate nor the metabolite demonstrated time-dependent inhibition of P450 2C9. The authors confirmed that the preincubation reaction was NADPH-dependent, therefore excluding the possibility that a reactive acyl-glucuronide (*11*) inactivated P450 2C8 via an apoprotein adduct. In addition, the inactivation followed normal Michaelis−Menten type kinetics in human liver microsomes, with a calculated K_I value (inhibitor concentration that supports half the maximal rate of enzyme inactivation) ranging from 20 to 52 *μ*M, depending on protein concentration, and a k_{inact} value (maximal rate of inactivation) of 0.21 min^{-1}. When time-dependent inhibition experiments were performed at two protein concentrations, differing by 10-fold, there was little change in the measured potency. This result indicated that product inhibition was not responsible for the observed time-dependent inhibition and, therefore, that GEM-1-*O*-gluc is an irreversible, mechanism-based inactivator of P450 2C8 (*10*).

The overall contribution of P450 2C8 irreversible inactivation by GEM-1-*O*-gluc to the observed GEM drug−drug interactions in the clinic is not entirely clear. Hinton et al. incorporated the time-dependent inhibition component due to GEM-1-*O*-gluc into a metabolic prediction model for the P450 2C8 substrates, cerivastatin, pioglitazone, repaglinide, rosiglitazone, and loperamide, and found that the predicted magnitude of drug−drug

* To whom correspondence should be addressed. Tel: 303-386-1185. E-mail: Brian.Baer@arraybiopharma.com.

[1] Abbreviations: AUC, area under the plasma drug concentration vs time curve; DLPC, L-α-dilauroylphosphatidylcholine; ESI, electrospray ionization; f_m, fraction metabolized; GEM, gemfibrozil; GEM-1-*O*-gluc, gemfibrozil-1-*O*-*β*-glucuronide; GEM-d_6-1-*O*-gluc, gemfibrozil-d_6-1-*O*-*β*-glucuronide; K_I, inhibitor concentration that supports half the maximal rate of inactivation; k_{inact}, maximal rate of enzyme inactivation; UGT, UDP-glucuronosyltransferase; UDPGA, uridine-5′-diphosphoglucuronic acid.

10.1021/tx900105n CCC: $40.75
Published on Web 05/15/2009

interaction was only marginally affected as compared to the prediction using reversible inhibition constants alone (*12*). Changes in predicted magnitude of interaction, due to irreversible inactivation, for cerivastatin [mean fold increase in area under the plasma drug concentration vs time curve (AUC) from 2.40 to 2.55] or repaglinide (mean fold increase in AUC from 1.89 to 1.97) were unable to account for the large interactions observed in the clinic (mean fold increase in AUC of 8.1 and 5.6, respectively). The authors argued that the irreversible component of GEM-1-*O*-gluc inhibition would significantly affect the prediction of drug−drug interactions only if the fraction metabolized (f_m) of the victim drugs by P450 2C8 was greater than 0.8 (*12*). The most pronounced GEM interactions have been observed with repaglinide (*2*) and cerivastatin (*1*), and these victim drugs are only partially metabolized by P450 2C8, with estimated $f_{m,P450\ 2C8}$ values of 0.61 and 0.49, respectively. Clinical pharmacokinetic interactions with GEM also may be explained, at least partially, by the inhibitory effects of GEM and its glucuronide on organic anion transporting polypeptide 2 (OATP2/OATP1B1) (*8, 12*) and GEM inhibition of UGT-mediated glucuronidation of victim drugs (*13*).

Despite the inability to account for the magnitude of drug−drug interactions by incorporating in vitro irreversible inhibition data, there is clinical evidence that supports a role for mechanism-based inhibition of P450 2C8 in the interaction between GEM and repaglinide. Tornio et al. reported that volunteers, who ingested 0.25 mg of repaglinide up to 12 h following a 600 mg dose of GEM, still demonstrated a significant increase in repaglinide plasma concentrations as compared to that observed in volunteers who ingested repaglinide and GEM simultaneously (*14*). At 12 h postadministration of GEM, plasma concentrations of GEM and its glucuronide were only 5−10% of their peak values (concentrations were similar and peaked at ∼30 μg/mL). Therefore, the authors argued that the long-lasting interaction is likely due to mechanism-based inhibition of P450 2C8 by GEM-1-*O*-gluc (*14*).

Mechanism-based inhibition of cytochrome P450 enzymes has been associated with the formation of metabolite−inhibitor complexes, covalent attachment of a reactive intermediate to the apoprotein, or modification of the heme prosthetic group (*15*). The pseudoirreversible bond formed between the metabolite and the heme group in metabolite−inhibitor complexes results from metabolism of secondary or tertiary nitrogen and therefore is not a viable mechanism for the irreversible inactivation of P450 2C8 by GEM-1-*O*-gluc. In the current study, mass analysis of a reaction mixture containing recombinant P450 2C8 and GEM-1-*O*-gluc revealed that the heme cofactor of P450 2C8, and not the apoprotein, was covalently modified during turnover. The structure of the GEM-1-*O*-gluc-heme adduct was characterized, and the mechanism of its formation was investigated.

Experimental Procedures

Materials. Alamethicin, amodiaquine, catalase, deuterium gas, GEM, GSH, labetalol, NADPH, palladium on carbon (10% Pd/C), D-saccharolactone, and uridine-5′-diphosphoglucuronic acid (UDPGA) were purchased from Sigma-Aldrich (St. Louis, MO). L-α-Dilauroylphosphatidylcholine (DLPC) was purchased from Avanti Polar Lipids Inc. (Alabaster, AL). *N*-Desethylamodiaquine and *N*-desethylamodiaquine-d_3 were purchased from BD Biosciences (San Jose, CA). Rat liver microsomes were purchased from CellzDirect, Inc. (Durham, NC). Deuterium oxide was from Cambridge Isotope Laboratories, Inc. (Andover, MA). Emulgen 911 was from Karlan Research Products Corp. (Cottonwood, AZ). Ni-NTA resin was from Qiagen (Valencia, CA). Complete protease inhibitor cocktail tablets were purchased from Roche Applied Science (Indianapolis, IN). Isopropyl-β-D-1-thiogalactopyranoside was from MoleculA (Columbia, MD). The pGro7 plasmid was from Takara Bio Inc. (Otsu, Shiga, Japan). A POROS R2 perfusion column (2.1 mm × 100 mm, 10 μm) was from Applied Biosystems (Cambridge, MA), Synergi Hydro-RP columns (2.0 mm × 250 mm, 4 μm, and 10 mm × 250 mm, 4 μm) and Luna phenyl-hexyl column (10 mm × 250 mm, 5 μm) were from Phenomenex (Torrance, CA), and a Supelco Acentis RP-amide column (2.1 mm × 50 mm, 3 μm) was from Sigma-Aldrich. HPLC grade acetonitrile and methanol were purchased from Mallinckrodt Baker, Inc. (Phillipsburg, NJ). The 3 and 20 mL Oasis HLB cartridges were purchased from Waters Corp. (Milford, MA).

Recombinant P450 2C8 and Coenzymes. Recombinant P450 2C8 was expressed using the pCW expression vector in *Escherichia coli* DH5α. Nucleotide substitutions were made at the N terminus to facilitate translation, resulting in the replacement of the first eight amino acid residues with MALLLAVF. The chaperones GroES and GroEL were coexpressed using the pGro7 vector. A culture was grown in 30 mL of Terrific Broth with 100 μg/mL carbenicillin and 20 μg/mL chloramphenicol in a 100 mL flask at 37 °C with shaking at 200 rpm. The following day, 10 mL of culture was transferred to a 4 L flask containing 1 L of Terrific Broth, trace elements (*16*), 100 μg/mL carbenicillin, 20 μg/mL chloramphenicol, and 5 mM thiamine. After the cells were incubated for 2 h at 37 °C, 4 g/L of arabinose was added to induce chaperone expression. Following an additional 2 h, P450 2C8 expression was induced with 1 mM isopropyl-β-D-1-thiogalactopyranoside, and 0.5 mM δ-aminolevulinic acid was added to facilitate heme biosynthesis. The temperature was reduced to 27 °C, and the cells were shaken at 180 rpm for 48 h. Pelleted cells were resuspended in 50 mM potassium phosphate buffer (pH 7.4) containing 500 mM NaCl, 20% glycerol, 50 μM amodiaquine, 20 mM β-mercaptoethanol, 1% Emulgen 911, and protease inhibitor cocktail tablets (1 tablet/50 mL). Cells were lysed using a French Press operated at 10000 psi, and cell lysates were then spun at 30000*g*. The supernatant was loaded directly onto Ni-NTA resin and equilibrated with 50 mM potassium phosphate buffer (pH 7.4), 500 mM NaCl, 20% glycerol, and 0.2% Emulgen 911. The column was washed with 200 mL of wash buffer containing 50 mM potassium phosphate buffer (pH 7.4), 20% glycerol, 20 mM imidazole, and 0.2% cholate. P450 2C8 was eluted from the column with buffer containing 50 mM potassium phosphate buffer (pH 7.4), 20% glycerol, 500 mM imidazole, and 0.2% cholate. The eluted protein was diluted to a concentration of approximately 15 μM, due to insolubility at high concentrations, and then dialyzed against 100 mM potassium phosphate, pH 7.4, in 20% glycerol and stored at −80 °C. Cytochrome b_5 and P450 reductase were expressed and purified as described previously (*17, 18*).

Mass Spectrometry. The following instrument setup was used for all LC/MS studies: HTS-PAL autosampler (Leap Technologies, Inc., Carrboro, NC), an Agilent 1200 Series HPLC with a diode array detector (Agilent Technologies Inc., Santa Clara, CA), and an API 4000 Q-trap triple quadrupole mass spectrometer (Applied Biosystems, Foster City, CA).

NMR Spectroscopy. NMR data were obtained with Varian, Inc. (Palo Alto, CA) Inova Spectrometer with a Varian Cold probe at 25 K and a cold preamplifier on the proton channel. ^{1}H NMR and ^{13}C NMR spectra were obtained at 500 and 100 MHz, respectively. All spectra were recorded in 120 μL of DMSO-d_6 in a "Bruker Tube" (2.5 mm id). Chemical shifts (δ) are expressed in ppm relative to the residual solvent peak (2.50 ppm). ^{1}H and ^{13}C had 90° pulse durations of 7.5 and 10.6 μs, respectively.

One-dimensional (1D) proton data collection was preformed with Varian's S2PUL sequence. ^{1}H NMR data were obtained with a 90° pulse duration of 7.5 μs, 1.892 s acquisition time, 4832 sweep width, 9143 complex points, with double precession sampling in real-time and a 2 s relaxation delay. These data were zero-filled to 64k with backward linear prediction with sb = 1.113 and sbs = −0.338 window functions. Water suppression was achieved with the

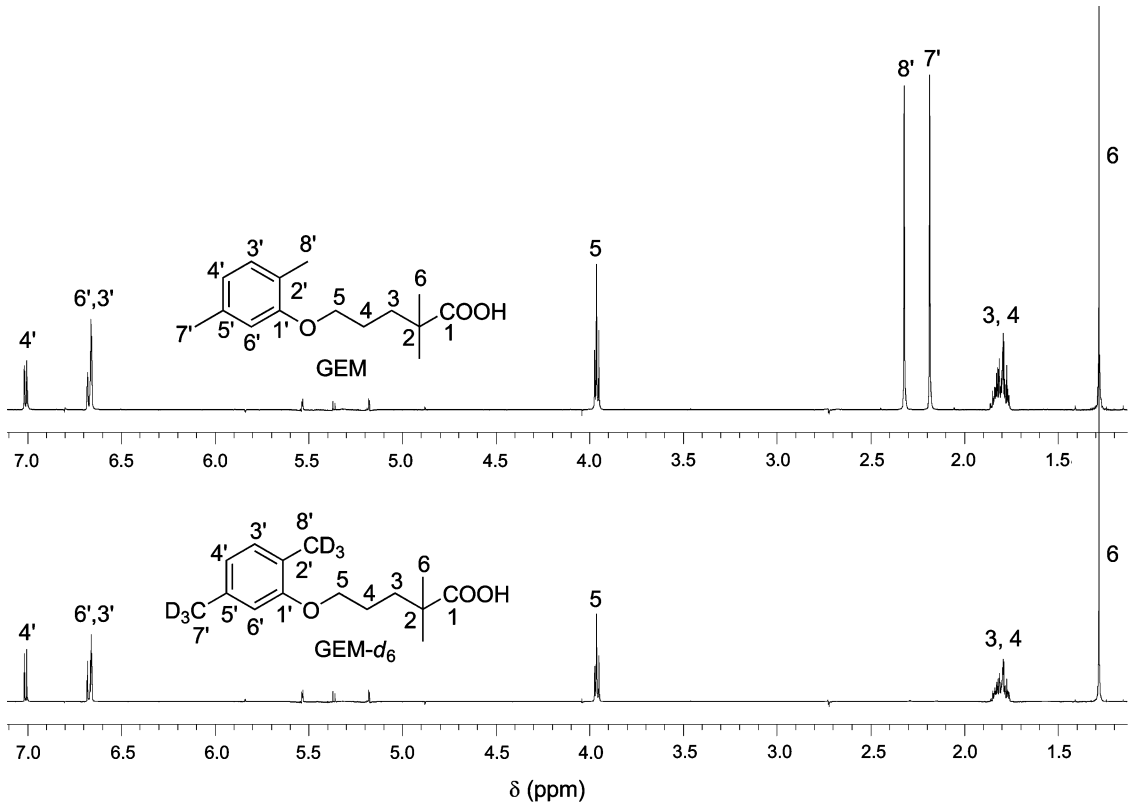

Figure 1. ^{1}H NMR spectra for GEM and GEM-d_6. The absence of methyl singlets H-8′ (2.32 ppm, s, 3H) and H-7′ (2.18 ppm, s, 3H) in the spectrum for GEM-d_6 indicated that deuterium was only exchanged at the benzylic positions.

PRESAT pulse sequence utilizing hard pulse saturation on water for 5 s, prior to S2PUL pulse train.

Nuclear Overhauser enhancement (NOE) experiments were measured using Varian's pulse program NOESY-1D, based on double pulsed field gradient spin echo nuclear Overhauser experiment (DPFGSE). Soft-shaped pulses were generated via Varian PBOX tools utilizing an "isnob2" pulse with 25.8 ms duration. The mixing time was set to 80 ms, and a 1.5 s relaxation delay was employed. The acquisition time was set to 1.896 s with a 4525 Hz spectral window. The data were "zero-filled" to 16k with backward linear prediction with a 0.3 GF window function.

Total correlation spectroscopy (TOCSY) experiments were obtained in one dimension utilizing Varian's pulse program TOCSY-1D. This is based upon HOHAHA pulse sequence with DPFGSE selection utilizing an "isnob2" soft-shaped pulse of 20 ms duration. A hard trim pulse of 2 ms was incorporated prior to spin lock via MELEV-17 of 80 ms at 7 kHz. The relaxation delay was set to 1.5 s with an acquisition time of 1.896 s with a sweep width of 4525 Hz. The data were "zero-filled" to 16k with backward linear prediction and a 0.3 GF window function.

Two-dimensional (2D) proton-carbon long-range cross-correlations were collected with the Varian gHMBCAD ^{1}H−^{13}C (gradient heteronuclear multiple bond correlation with adiabatic decoupling) and gHSQC ^{1}H−^{13}C (gradient heteronuclear single quantum correlation with adiabatic decoupling) pulse sequences. ^{1}H and ^{13}C spectral widths of 4832 and 30000 Hz were centered at 5.0 and 99 ppm, respectively. A total of 1200 scans of 1024 complex points were collected for each of the 160 t_1 increments. The one-bond J filter was set to 3.5714 ms ($^1J_{H,C}$ = 140 Hz) and the "n" bond J filter was set to 62.5 ms ($^1J_{H,C}$ = 8 Hz). A recovery delay of 1.2 s was used prior to each scan, and the total acquisition time was 69 h. The spectra were transformed after zero filling to 2048 × 2048 complex points, and a $\pi/3$ shifted sinebell square was used as a window functions. Gradient selection was set to 10 gauss/cm for 2 ms with gradient recovery time of 0.5 ms. Crusher gradients were set to 10 gauss/cm for 1.6 ms, and adiabatic pulses were created with a WURST2i pulse over 43000 Hz with a pulse width of 465.4 μs.

Synthesis of GEM-d_6. The hydrogen atoms on both benzylic carbons of GEM were selectively exchanged with deuterium using Pd/C and D_2 gas as described by Sijiki et al. (*19*). GEM (150 mg) and 10% Pd/C (15 mg) were dissolved in 50 mM sodium carbonate buffer in D_2O, and the pH was adjusted to 8.0 with concentrated HCl. The solution was bubbled with deuterium gas for 30 s, sealed in a 15 mL pressure tube, and heated at 150 °C for 24 h. An additional 15 mg of 10% Pd/C was added, deuterium gas was again bubbled through the solution, and it was heated at 150 °C for another 6 h. Deuterium incorporation was monitored by LC/MS [electrospray ionization (ESI−)], and the reaction was deemed complete when the mass for GEM had shifted from *m/z* 249 to *m/z* 255, with minimal contribution from partially labeled compound. Exclusive fragmentation of *m/z* 255 to *m/z* 127 in the MS^2 spectrum confirmed that the six deuterium atoms were confined to the 2′,5′-dimethylphenoxy group. The solution was diluted with 80 mL of H_2O and acidified with 1 mL of 1 M HCl, and GEM-d_6 was extracted with 50 mL of dichloromethane. The solvent was evaporated using a rotary evaporator, and the regiospecificity of stable label incorporation into the 2′,5′-dimethylphenoxy group of GEM was confirmed by NMR. The ^{1}H and ^{13}C NMR signal assignments of GEM and GEM-d_6 were achieved using chemical shift, spin−spin coupling, and through-space NOE information obtained from the proton and carbon domain, as well as one bond and three bond information from 2D cross-correlation (^{1}H−^{13}C) experiments (gHSQC and gHMBCAD). Because the ^{1}H detection domain was observed at 500 MHz and deuterium (^{2}H) would have resonated at 76 MHz, the distinct absence of methyl singlets, representing protons on the benzylic carbons C-8′ (2.32 ppm, s, 3H) and C-7′ (2.18 ppm, s, 3H), confirmed full deuterium incorporation (>99.5%) at these positions (Figure 1). Furthermore, integration of ^{1}H data, collected with long T_1 relaxation (60 s), indicated that protons had not been exchanged with deuterium at any other position on GEM.

Biosynthesis of GEM-1-*O*-gluc and Gemfibrozil-d_6-1-*O*-β-glucuronide (GEM-d_6-1-*O*-gluc). GEM or GEM-d_6 (4 mM) was incubated with rat liver microsomes (1 mg protein/mL), alamethicin (0.1 mg/mL), D-saccharolactone (10 mM), and UDPGA (4 mM)

in 40 mL of 50 mM potassium phosphate buffer (pH 7.4) for 8 h at 37 °C. The reaction mixture was acidified with 1% formic acid, and GEM-1-*O*-gluc and GEM-d_6-1-*O*-gluc were extracted with 2 × 40 mL of ethyl acetate. The organic layer was evaporated to dryness under nitrogen, and the remaining residue was dissolved in 1.5 mL of DMSO:acetonitrile:water (1:1:2 by volume). This solution was loaded onto a phenyl-hexyl semipreparative column (10 mm × 250 mm, 5 μm), which was equilibrated with 80% mobile phase A (0.1% formic acid and 1% isopropanol in H_2O) and 20% mobile phase B (0.1% formic acid in acetonitrile), at a flow rate of 3.5 mL/min. Mobile phase B was increased to 95% over 15 min, held at 95% for 2 min, returned to 20% over 0.5 min, and held at 20% for 2.5 min prior to the next injection. Under these conditions, GEM-1-*O*-gluc (or GEM-d_6-1-*O*-gluc) eluted at 12.2 min, as determined by absorbance at 275 nm (A_{275}) and MS analysis. GEM-1-*O*-gluc or GEM-d_6-1-*O*-gluc elution was monitored subsequently by A_{275}, and the corresponding peaks in the chromatograms were collected from six injections of 250 μL of each solution. The pooled fractions were dried under nitrogen. The final yields were 26.9 mg of GEM-1-*O*-gluc and 27.9 mg of GEM-d_6-1-*O*-gluc. Each compound was dissolved in DMSO to make 100 mM stock solutions.

Reconstitution of Recombinant P450 2C8. The previously isolated recombinant P450 2C8 (0.5 μM) was combined with P450 reductase (1 μM) at room temperature for 10 min. DLPC (20 μg/mL) was added and followed 5 min later by cytochrome b_5 (0.5 μM). After a total of 20 min, GSH (3 mM) and catalase (500 units/mL) were added, and the volume was adjusted with 50 mM potassium phosphate (pH 7.4). Substrate was added, and the reconstituted P450 2C8 solution was incubated for 15 min at 37 °C prior to reaction initiation with NADPH (1 mM). To confirm the activity of P450 2C8, kinetic parameters were determined for amodiaquine metabolism, using a similar reconstituted reaction mixture containing 1 pmol of P450 2C8, 2 pmol of P450 reductase, and 1 pmol of cytochrome b_5. The calculated K_m was 1.95 ± 0.07 μM, and the k_{cat} was 6.87 ± 0.07 pmol/pmol P450/min. These values agreed well with the activity of recombinant P450 2C8 in microsomes (heterologously expressed in Sf9 cells) toward amodiaquine (K_m = 0.728 ± 0.040 μM and k_{cat} = 11.2 ± 0.2 pmol/pmol P450/min) (*20*).

Time-Dependent Inactivation Studies with GEM-1-*O*-gluc. Twelve 200 μL primary reactions were incubated with GEM-1-*O*-gluc or GEM-d_6-1-*O*-gluc (final concentrations ranging from 10 to 600 μM obtained by diluting DMSO stock solutions 1:100) in a 96 well plate heated to 37 °C by a Jitterbug (Boekel Scientific, Feasterville, PA). At 4 min intervals, ranging from 0 to 24 min, and at 90 min (for calculation of partition ratio), 4 μL of the primary reaction was transferred to a 196 μL secondary reaction (1:50 dilution) containing amodiaquine (20 μM) and NADPH (1 mM) in 50 mM potassium phosphate buffer (pH 7.4). The secondary reaction was allowed to proceed for 10 min at 37 °C and then quenched with 20 μL of aqueous 50% formic acid. After all of the reactions were quenched, the internal standard, *N*-desethylamodiaquine-d_3 (0.5 μM final), was added, and proteins were precipitated by the addition of an equal volume of acetonitrile. Following centrifugation, 125 μL aliquots of each sample were transferred to another 96 well plate for LC/MS (ESI+) analysis of the *N*-desethylamodiaquine metabolite. Samples (10 μL) were injected onto a RP-amide column (2.1 mm × 50 mm, 3 μm) equilibrated with 98% mobile phase C (10 mM ammonium acetate and 0.1% formic acid in water) and 2% of mobile phase B (0.1% formic acid in acetonitrile) flowing at 0.8 mL/min. Mobile phase B was held at 2% for 0.2 min, increased to 90% over 1.3 min, held at 90% for 0.5 min, returned back to 2% over 0.1 min, and held at 2% for 1.4 min prior to the next injection. Under these conditions, *N*-desethylamodiaquine (*m/z* 328 → *m/z* 283) and *N*-desethylamodiaquine-d_3 (*m/z* 331 → *m/z* 283) both eluted at 1.7 min. The concentrations of *N*-desethylamodiaquine in the samples were determined by measuring the ion chromatogram peak area for *N*-desethylamodiaquine, relative to that of the internal standard, and comparing the values to a calibration curve generated with known *N*-desethylamodiaquine concentrations. The reaction rates were calculated from the negative slope of the log-transformed percent P450 2C8 activity vs time plots for each inhibitor concentration. Rates of inactivation (λ) were plotted against the inhibitor concentration, and the data were fitted by nonlinear regression using Sigma Plot 9.0 (Systat Software, Inc., San Jose, CA) according to the following equation (*21*):

$$\lambda = \frac{k_{inact} \times [I]}{K_I + [I]} \quad (1)$$

In this equation, λ represents the rate constant for inactivation at each inhibitor concentration, [I] is the inhibitor concentration, K_I is the inhibitor concentration that produces half the maximal rate of inactivation, and k_{inact} represents the maximal rate of inactivation. The partition ratio was determined using the substrate depletion method (*21*). Inactivation rates were plotted against [I]/[enzyme], and the initial linear portion of the curve was projected to the *x*-axis to obtain the turnover number. The partition ratio was calculated by subtracting one from the turnover number.

Analysis of Modified Heme. The primary reaction was conducted as described above (reaction of P450 2C8 with GEM-1-*O*-gluc) except that catalase was omitted. Preliminary experiments revealed that catalase did not have an effect on GEM-1-*O*-gluc-heme adduct formation, so it was eliminated from the reaction due to its contribution to total heme quantification. A 500 μL reaction was incubated for 0, 4, 8, 16, and 24 min, time intervals that corresponded to the points in the time-dependent inhibition study. The reaction was quenched with 1% aqueous formic acid, and the entire solution was injected directly onto a POROS R2 column and equilibrated with 80% mobile phase D (0.1% TFA in water) and 20% mobile phase E (0.1% TFA in acetonitrile) flowing at 0.5 mL/min. Mobile phase E was held at 20% for 1 min, increased to 56% over 16 min, held at 56% for 4 min, increased to 95% over 3 min, held at 95% for 3 min, returned to 10% over 0.5 min, and held at 20% for 2.5 min prior to the next injection. Heme eluted at 12.0 min, the GEM-1-*O*-gluc-heme adduct eluted at 14.1 min, and P450 2C8 apoprotein eluted at 22.0 min, as determined by UV/vis absorbance, MS (ESI+), and MS^2. The declustering potential was set at 65 for all experiments, and the collision energy was set at 45 with a collision energy spread of 15 for MS^2 experiments of the GEM-1-*O*-gluc-heme adduct.

Characterization of GEM-1-*O*-gluc Metabolites. To qualitatively compare metabolite profiles, 1 mL aliquots of the primary reaction with saturating concentrations of GEM-1-*O*-gluc or GEM-d_6-1-*O*-gluc were incubated for 90 min at 37 °C. Labetalol (4 μM) was added as an internal standard, and metabolites were extracted using solid-phase extraction (3 mL Oasis HLB cartridge). The cartridge was conditioned by washing it with methanol and subsequent equilibration with H_2O prior to loading the sample. Once the sample was loaded, the cartridge was washed with 5% methanol in H_2O and eluted with acetonitrile. The acetonitrile eluate was dried under nitrogen, and the residue was dissolved in 100 μL of 50% acetonitrile in 1 mM ammonium carbonate (pH 7.4) and kept on melting ice until purification. Samples were injected onto a Synergi Hydro-RP column (2.0 mm × 250 mm, 4 μm), equilibrated with 80% mobile phase A (0.1% formic acid and 1% isopropanol in H_2O) and 20% mobile phase F (0.1% formic acid and 50% methanol in acetonitrile) flowing at 0.3 mL/min. Mobile phase F was increased to 80% over 30 min, then increased to 95% in 5 min, held at 95% for 3 min, returned to 20% over 0.1 min, and held at 20% for 7 min prior to the next injection. Metabolite M1 eluted at 20.8 min, metabolite M2 eluted at 21.3 min, metabolite M3 eluted at 21.7 min, and GEM-1-*O*-gluc eluted at 29.7 min, as determined by A_{275} (bandwidth of 30), MS (ESI−), and MS^2.

To obtain enough material for structural assignment by NMR, metabolites were extracted from a 20 mL reaction using a 20 mL HLB cartridge and purified on a semipreparative version of the Hydro-RP column (10 mm × 250 mm, 4 μm). The column was equilibrated with 80% mobile phase A and 20% mobile phase F,

flowing at 2.5 mL/min. Mobile phase F was increased to 95% over 30 min, held at 65% for 2 min, returned to 20% over 0.5 min, and held at 20% for 6 min prior to the next injection. Metabolite M1 eluted at 22.1 min, metabolite M2 eluted at 22.5 min, and metabolite M3 eluted at 23.0 min on this column. The three metabolites were monitored by A_{275} and collected individually from six injections of 250 μL each. Ammonium bicarbonate (pH 7.4, 50 mM) was added to fractions containing metabolite M1 in an attempt to prevent degradation. The pooled fractions for each metabolite were dried under nitrogen, and the remaining residue was dissolved in 0.5 μL of DMSO-d_6 for NMR spectra acquisition. The residue containing metabolite M1 was dissolved in D_2O, loaded, washed, and eluted from a 3 mL HLB cartridge to remove the buffer salts, dried again, and finally dissolved in DMSO-d_6.

Modeling of GEM-1-*O*-gluc in the P450 2C8 Active Site. Five structures of human P450 2C8 were available through the RCSB Protein Data Bank (www.pdb.org) with accession codes 1PQ2, 2NNH, 2NNI, 2NNJ, and 2VN0. All five structures were downloaded and aligned. Given the flexibility of the P450 2C8 binding site, three structures (1PQ2, 2NNH, and 2NNI) were selected that provided complete coverage of structural differences as well as eliminating as many structural defects (e.g., strand breaks) as possible. Structures were prepared for computational docking studies using the molecular modeling software suite, Maestro version 8.5.207. GEM-1-*O*-gluc was constructed within Maestro and energy minimized to a reasonable low-energy conformation using MacroModel 9.6 and the OPLS-2005 force field. The small molecule was independently docked into the prepared protein structures using Glide, version 5.0, using SP (Standard Precision) Scoring and no imposed constraints. All computational tools are components of the Schrodinger Software Suite (Schrodinger, Inc., New York, NY).

Results

Identification of Modified Heme. Preliminary experiments were designed to determine if P450 2C8 was inactivated by GEM-1-*O*-gluc via covalent binding to the apoprotein or GEM-1-*O*-gluc-heme adduct formation. Recombinant human P450 2C8 was reacted with 100 μM GEM-1-*O*-gluc for 24 min and then loaded onto a POROS R2 column for LC/UV/vis and MS analysis of both the apoprotein and the heme. The peak representing P450 2C8 in the A_{280} chromatogram was analyzed by MS, but the deconvoluted whole protein mass spectrum did not reveal any modification of P450 2C8 following inactivation by GEM-1-*O*-gluc (data not shown). The UV/vis chromatogram then was analyzed for any peaks that absorbed in the 400 nm region that could represent changes in the heme profile vs the control reaction. In fact, the signal intensity representing heme at 12.0 min had reduced, and a new peak was observed at 14.1 min (Figure 2). The electronic absorption spectrum of the GEM-1-*O*-gluc- and NADPH-dependent peak revealed that the λ_{max} was red-shifted to 407 nm as compared to unmodified heme with a λ_{max} of 399 nm (Figure 3). Absorption maxima also were observed at 509 and 636 nm for the GEM-1-*O*-gluc-heme adduct, as compared to 502 and 627 nm for native heme. Mass spectrometry (ESI+) showed that the modified heme had an *m*/*z* value of 1040.7, consistent with the addition of 1 equiv of GEM-1-*O*-gluc (+426 amu) to heme (616 amu) and the loss of two hydrogen atoms (−2 amu). The MS spectrum at 14.1 min, filtered with a neutral loss scan of −*m*/*z* 176 (glucuronide), is shown in Figure 4A. Subsequent MS^2 analysis revealed only one major fragment ion, *m*/*z* 864, representing the loss of the glucuronide moiety (Figure 4B). For additional structural confirmation, MS^3 experiments were performed on the *m*/*z* 864 fragment ion, and the resulting spectrum is shown in Figure 4C. Cleavage at the ether linkage resulted in the diagnostic fragment of *m*/*z* 736, which demonstrates that GEM-1-*O*-gluc is attached to the heme via the 2′,5′-dimethylphenoxy group.

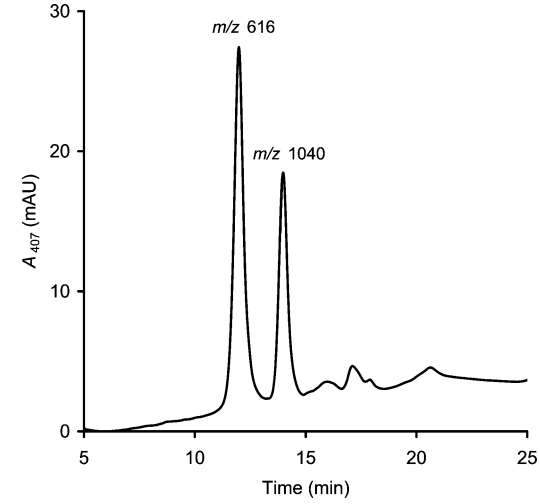

Figure 2. HPLC profile of intact heme and the heme adduct resulting from the oxidation of GEM-1-*O*-gluc by P450 2C8. Corresponding *m*/*z* values were determined by electrospray ionization mass spectrometry (ESI+).

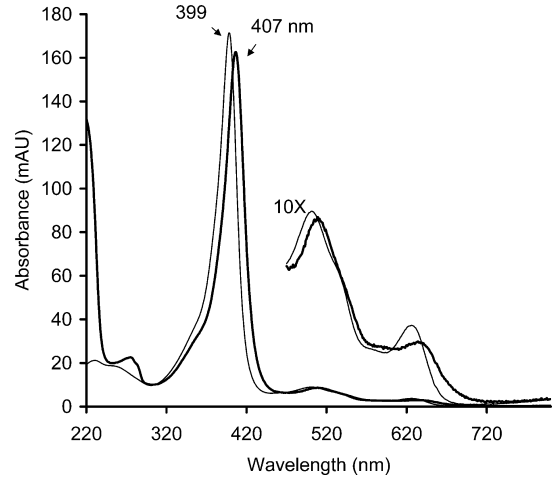

Figure 3. Electronic absorption spectrum for heme and the GEM-1-*O*-gluc-heme adduct. Absorption maxima for the native heme (thin trace) and modified heme (bold trace) are 399 and 407 nm, respectively, in approximately 50% aqueous acetonitrile containing 0.1% TFA. The spectra are magnified 10-fold from 470 to 800 nm.

Fragment ions *m*/*z* 615 and *m*/*z* 616 were formed presumably by the complete cleavage of GEM-1-*O*-gluc from the GEM-1-*O*-gluc-heme adduct, to give a heme radical ion and heme, respectively. The heme fragment ion *m*/*z* 569 may have resulted from a neutral loss of formic acid from the propionate group of the heme radical ion (*m*/*z* 615 minus *m*/*z* 46), and the fragment ion *m*/*z* 542 may have formed from a neutral loss of propionic acid from the heme (*m*/*z* 616 minus *m*/*z* 74).

Reaction of GEM-d_6-1-*O*-gluc with P450 2C8. An analogue of GEM-1-*O*-gluc, containing deuterium atoms on both benzylic methyl groups, was synthesized to probe the mechanism of GEM-1-*O*-gluc-heme adduct formation and help distinguish between various isomeric structures. The GEM-d_6-1-*O*-gluc analogue was reacted with P450 2C8, and the sample was analyzed by MS to evaluate the number of deuterium atoms retained in the modified heme. The observed *m*/*z* of 1045.7 indicates that that one of the original six deuterium atoms of GEM-d_6-1-*O*-gluc was lost upon heme adduct formation (Figure 4D). The MS^2 and MS^3 spectra confirm that the *m*/*z* shift, due to the five remaining deuterium atoms, was confined to the 2′,5′-dimethylphenoxy group, attached to the heme (Figure 4E,F).

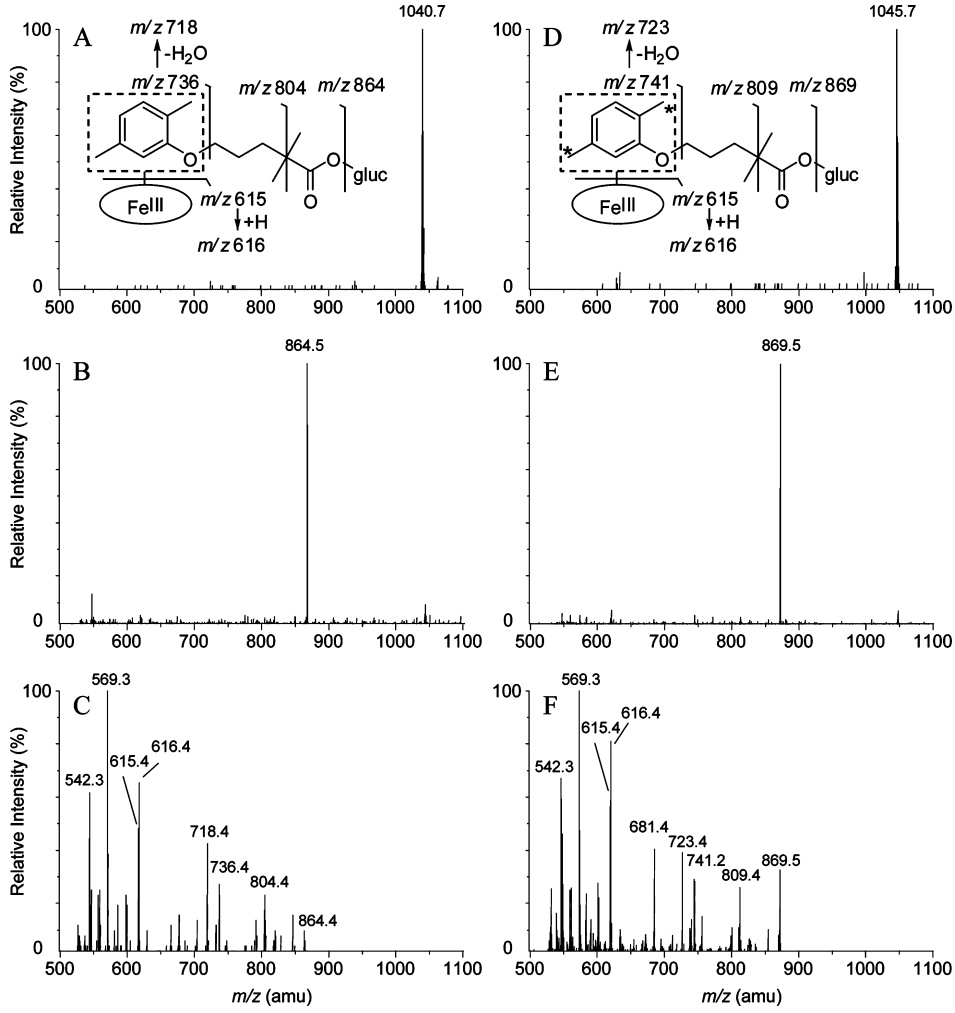

Figure 4. Mass spectra of the GEM-1-*O*-gluc- and GEM-d_6-1-*O*-gluc-heme adducts. (A) MS spectrum acquired at 14.1 min corresponding to the peak in the A_{407} chromatogram shown in Figure 2, (B) MS^2 spectrum of *m*/*z* 1040, (C) MS^3 spectrum of *m*/*z* 864, (D) MS spectrum of GEM-d_6-1-*O*-gluc-heme adduct, (E) MS^2 spectrum of *m*/*z* 1045, and (F) MS^3 spectrum of *m*/*z* 869. The "*" on the GEM-d_6-1-*O*-gluc-heme adduct structure designates the benzylic positions that originally contained three deuterium atoms each.

Time Course of GEM-1-*O*-gluc-Heme Adduct Formation. Saturating concentrations (400 μM) of GEM-1-*O*-gluc or GEM-d_6-1-*O*-gluc were reacted with P450 2C8 for various time intervals, and the relative levels of native heme and GEM-1-*O*-gluc-heme adduct were monitored by LC/UV/vis. The normalized peak area due to each heme in the A_{407} trace was plotted vs time in Figure 5. Following the reaction of P450 2C8 with GEM-1-*O*-gluc, an initial rapid increase in the 407 nm-absorbing peak, representing the GEM-1-*O*-gluc-heme adduct, was observed in the first 4 min, and then, the rate of formation appeared to decrease. There was no further change in the amount of GEM-1-*O*-gluc-heme adduct between 16 and 24 min. Formation of the GEM-1-*O*-gluc-heme adduct was not well-represented with first-order reaction kinetics, and so, reaction rates were not calculated. After a 24 min reaction with GEM-1-*O*-gluc, the A_{407} peak area representing GEM-1-*O*-gluc-heme adduct was approximately 12% of the A_{407} peak area due to native heme at 0 min. Concentrations relative to native heme were not estimated because the change in extinction coefficient upon heme alkylation is unknown. Under identical conditions, the A_{407} peak area representing GEM-d_6-1-*O*-gluc-heme adduct was approximately 7% of the A_{407} peak area due to native heme at 0 min, demonstrating a 1.7-fold decrease in heme adduct formation due to deuterium substitution. Interestingly, the apparent rapid loss of native heme was similar in reactions of P450 2C8 with both GEM-1-*O*-gluc and GEM-d_6-1-*O*-gluc at all time points. Relative to the control reaction with amodiaquine, P450 2C8 reactions with GEM-1-*O*-gluc and GEM-d_6-

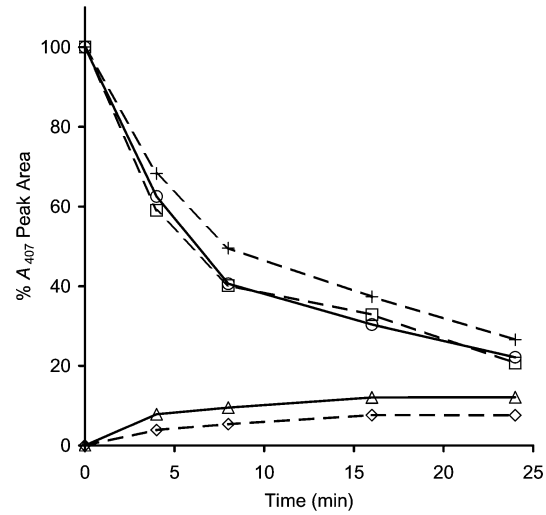

Figure 5. Changes in the heme profile of P450 2C8 during the reaction with GEM-1-*O*-gluc. The loss of the native heme chromophore in the reaction with GEM-1-*O*-gluc (○) or GEM-d_6-1-*O*-gluc (□) and the formation of the GEM-1-*O*-gluc-heme adduct chromophore in the reaction with GEM-1-*O*-gluc (△) or GEM-d_6-1-*O*-gluc (◇) were monitored over 24 min. The heme chromophore loss also was monitored in a control reaction with amodiaquine (+).

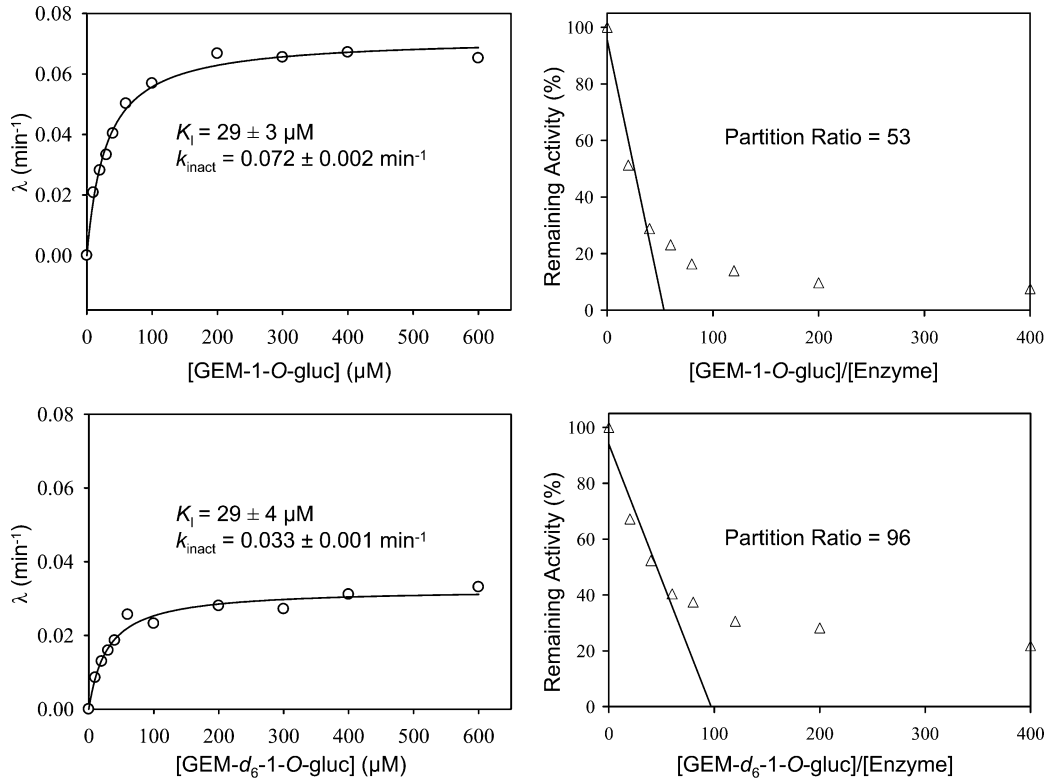

Figure 6. Determination of K_I, k_{inact}, and the partition ratio for the inactivation of P450 2C8 by GEM-1-*O*-gluc and GEM-d_6-1-*O*-gluc. The first-order inactivation rate is represented by "λ".

1-*O*-gluc resulted in slightly greater loss of the native heme chromophore. Incomplete loss of native heme following the 24 min reaction may be partly due to the contribution of heme from the coenzyme, cytochrome b_5. The modified heme could still be generated in a reaction without cytochrome b_5, but the rate of formation was slower (data not shown).

Time-Dependent Inhibition Kinetics and Partition Ratio. A time-dependent inhibition kinetic analysis was performed with P450 2C8 and either GEM-1-*O*-gluc or GEM-d_6-1-*O*-gluc to determine if hydrogen atom abstraction at the benzylic position was the rate-limiting step in the mechanism of inactivation. Following preincubation of P450 2C8 with concentrations of GEM-1-*O*-gluc or GEM-d_6-1-*O*-gluc ranging from 0 to 600 μM, for various time intervals from 0 to 24 min, the remaining activity was monitored by turnover of amodiaquine to *N*-desethylamodiaquine. First-order inactivation rates (λ) were plotted vs concentration, and the K_I and k_{inact} values were determined using nonliner regression (Figure 6). The calculated K_I values for GEM-1-*O*-gluc (29 $\pm$ 3 μM) and GEM-d_6-1-*O*-gluc (29 $\pm$ 4 μM) were similar, but the maximum inactivation rate, k_{inact}, of P450 2C8 by GEM-d_6-1-*O*-gluc (0.033 $\pm$ 0.001 min^{-1}) was 2.2-fold slower than the k_{inact} determined with GEM-1-*O*-gluc (0.072 $\pm$ 0.002 min^{-1}).

The partition ratio, which is a measure of turnover events per inactivation event, was calculated by the substrate depletion method (*21*). P450 2C8 was reacted with GEM-1-*O*-gluc or GEM-d_6-1-*O*-gluc at concentrations ranging from 0 to 600 μM for 90 min, prior to measurement of remaining amodiaquine *N*-desethylation activity. No additional inactivation of P450 2C8 was observed at a 2 h time point (data not shown). The remaining activity was plotted vs [GEM-1-*O*-gluc]/[enzyme], and the initial linear portion of the curve was projected to the *x*-axis to obtain the turnover number (Figure 6). The partition ratio, which is equal to the turnover number minus one, between P450 2C8-dependent metabolism and P450 2C8 inactivation was calculated to be 53 with GEM-1-*O*-gluc as the substrate as compared to 96 with GEM-d_6-1-*O*-gluc as the substrate.

Characterization of GEM-1-*O*-gluc and GEM-d_6-1-*O*-gluc Metabolites. The increase in partition ratio due to deuterium labeling of the methyl groups of GEM-1-*O*-gluc indicated that metabolic switching has occurred. To identify the sites of oxidation, metabolite profiles resulting from the P450 2C8 reaction with GEM-1-*O*-gluc or GEM-d_6-1-*O*-gluc were examined following complete inactivation with saturating concentrations of substrate. Three metabolites of GEM-1-*O*-gluc, M1, M2, and M3, were detected in the A_{275} chromatogram when the samples were analyzed on a Polar-RP column (Figure 7A). The corresponding MS spectra for all peaks revealed a molecular ion of *m*/*z* 441, with negative ionization (+*m*/*z* 16 amu relative to *m*/*z* 425 for GEM-1-*O*-gluc), indicating that three single oxidations of GEM-1-*O*-gluc had occurred. Fragment ions present in the MS^2 spectra of all three metabolites indicated that oxidation had occurred on the 2′,5′-dimethylphenoxy group (Table 1), and the fragmentation patterns agreed with MS^2 data previously acquired (*10*). Concentrations of metabolites M1, M2, and M3 (designated according to retention time) were compared by measuring the peak area in the A_{275} chromatogram relative to the peak area of the internal standard, labetalol. The calculated area ratios for M1, M2, and M3 were 0.64 $\pm$ 0.12, 2.74 $\pm$ 0.05, and 0.81 $\pm$ 0.02, respectively. The metabolite profile also was examined following the reaction of P450 2C8 with saturating concentrations of GEM-d_6-1-*O*-gluc (Figure 7B). Metabolite M1 had a molecular ion at *m*/*z* 447, indicating that all deuterium atoms were retained, whereas M2 and M3 had molecular ions at *m*/*z* 446, suggesting that one deuterium atom was lost upon oxidation. After complete inactivation of P450 2C8 by GEM-d_6-1-*O*-gluc, the peak area ratio of M1 (4.24 $\pm$ 0.43) was more than 6-fold higher than observed with GEM-1-*O*-gluc, whereas the peak area ratios for M2 (2.38 $\pm$ 0.18) and M3 (1.05 $\pm$ 0.09) were approximately the same.

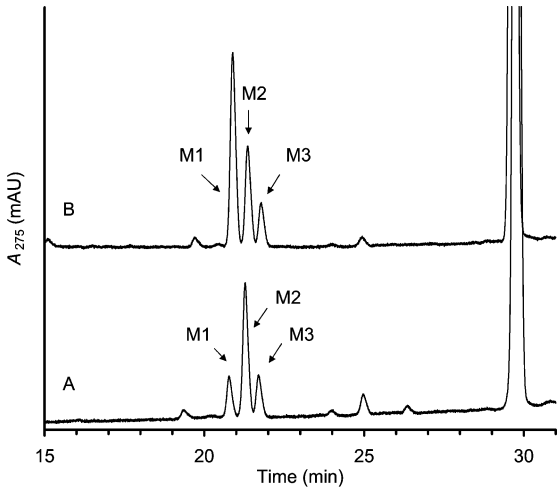

Figure 7. HPLC profile of metabolites formed upon oxidation of GEM-1-*O*-gluc or GEM-d_6-1-*O*-gluc by P450 2C8. Metabolites were evaluated following complete inactivation of P450 2C8. (A) Metabolites formed from GEM-1-*O*-gluc. (B) Metabolites formed from GEM-d_6-1-*O*-gluc.

Initial metabolite identification experiments demonstrated that M1 was not stable in acetonitrile and water (50:50), which was used to resuspend metabolites for LC/MS analysis. A decrease in the relative amount of M1, as compared to the other metabolites, was observed upon repeat injections, and the metabolite was not detectable by A_{275} when left at room temperature overnight. Interestingly, a new peak with a retention time of 5.1 min was detected when a neutral loss scan of *m*/*z* 176 was performed. The corresponding *m*/*z* value was 321, and subsequent fragmentation confirmed an *m*/*z* value of 145 (loss of glucuronide) in the MS^2 spectrum. These data indicated that M1 chemically degraded via cleavage at the ether linkage. Degradation was apparently pH-dependent, because the reaction could be slowed with the addition of 1 mM ammonium bicarbonate (pH 7.4) to the metabolite mixture that was eluted following solid-phase extraction.

Metabolites of GEM-1-*O*-gluc were biosynthesized in a large reaction with P450 2C8, chromatographically purified, and analyzed by NMR for structure assignment. The NMR analysis of GEM-1-*O*-gluc metabolites, M1, M2, and M3, was initially approached by inspection of their spin−spin couplings, within their respective aromatic systems. Metabolites M2 and M3 displayed the aromatic ABX spin system that was observed with parent GEM. Dissimilarly, the aromatic spin system of M1 was observed as an AX spin system. This observation for M1, in combination with NOE and 2D gHMBCAD $^1H-^{13}C$ experimental data, mandated the site of hydroxylation at C-4′. Therefore, metabolite M1 was assigned as 4′-hydroxy-GEM-1-*O*-gluc (Table 1). With regard to M2 and M3, the ^1H domain observational change for one of the two aromatic methyl singlets indicated that hydroxylation had occurred at benzylic positions. To differentiate between the two regioisomers, the benzylic methylene groups on M2 and M3 were each preirradiated in 1D NOESY experiments, and the observed enhancements were evaluated. Preirradiation of M2-methylene protons at 4.43 ppm demonstrated enhancement at AB − H-6′ (6.87 ppm, d, $J = 2$ Hz) and H-4′ (6.75 ppm, dd, $J = 7.5$ Hz, 2 Hz); therefore, the metabolite was designated GEM-1-*O*-gluc-5′-benzyl alcohol (Table 1). When the M3-methylene protons at 4.46 ppm were preirradiated, enhancement was observed at X − H-3′ (7.22 ppm, d, $J = 8.3$ Hz), and the metabolite was designated GEM-1-*O*-gluc-2′-benzyl alcohol (Table 1). Furthermore, gHMBCAD − $^1H-^{13}C$ data revealed the expected proton-carbon connectivity and carbon chemical shifts that were consistent with these assigned structures (Table 1). Proton chemical shift assignments for these GEM-1-*O*-gluc metabolites agree well with the chemical shifts previously assigned to metabolites characterized in the urine of Sprague−Dawley rats, following an orally administered dose of GEM (*22*).

Computational Docking Studies of GEM-1-*O*-gluc in P450 2C8. Given the availability of crystal structures for P450 2C8, computational docking studies were performed to investigate heme adduct formation from a structural perspective. Crystal structures of P450 2C8 and GEM-1-*O*-gluc were prepared as described in the Experimental Procedures, and docking was performed with no constraints imposed upon ligand orientation apart from those provided by the structure of P450 2C8 itself. Given the flexibility of GEM-1-*O*-gluc and the size of the active site of P450 2C8, docking parameters were set to return the 10 top-scoring poses identified. By evaluating multiple putative binding modes, an assessment could be made with regard to the reproducibility of the docking process as well as to establish a degree of confidence in those identified putative docking modes. Obviously, if no consensus could be identified among multiple binding modes, little confidence could be assigned to the result. To further challenge the docking process, multiple structures for P450 2C8 were utilized, and docking maneuvers were performed with each one independently, again seeking a degree of consensus.

Within each docking experiment utilizing a particular crystal structure, a strong consensus was seen for the overall orientation of GEM-1-*O*-gluc within the active site of P450 2C8 with the 2′,5′-dimethylphenoxy group being positioned directly above the heme functionality of the enzyme. The glucuronide moiety consistently was directed toward the N terminus of helix B′ but tended to exhibit much more flexibility in its location. In the majority of docking results, hydrogen-bonding interactions would be expected with one or more of the polar residues in this region of the active site, such as Asn99, Ser103, Gln214, and Asn217. Docking results between crystal structures, despite changes in the active site geometry between structures, were consistent in overall positioning of GEM-1-*O*-gluc in the P450 2C8 active site, in positioning of the 2′,5′-dimethylphenoxy group above the heme and in the orientation of the glucuronide moiety toward the N terminus of helix B′ (Figure 8). Strikingly, the position of the 2′,5′-dimethylphenoxy group was maintained as well between groups as within results for a single, particular crystal structure. One of the benzyl groups of GEM-1-*O*-gluc was positioned consistently within 3.0−4.0 Å of the γ-meso position of the heme. Neither benzylic carbon (2′- or 5′-position), however, preferentially was found in this location as rotameric changes could be easily accommodated by the flexible alkyl chain of GEM-1-*O*-gluc. Despite the flexibility of GEM-1-*O*-gluc, steric constraints imposed by P450 2C8 prevented either benzylic carbon from orienting near either of the heme vinyl groups, suggesting that they would not be accessible for adduct formation with GEM-1-*O*-gluc.

Discussion

The chemical structure of GEM-1-*O*-gluc lacks an obvious metabolic liability, such as a furan, thiophene, acetylene, or terminal alkene group, that may be bioactivated (*15*) and, consequently, result in mechanism-based inactivation of P450 2C8. Ogilvie et al. detected an oxidized metabolite of GEM-1-*O*-gluc in incubations with human liver microsomes and therefore hypothesized that aromatic hydroxylation on the 2′,5′-dimethylphenoxy group of GEM-1-*O*-gluc, and subsequent

Table 1. Structural Characterization of Metabolites Formed from the Reaction of GEM-1-*O*-gluc with P450 2C8

Metabolite	M1 4′-hydroxy-GEM-1-*O*-gluc		M2 GEM-1-*O*-gluc-5′-benzyl alcohol		M3 GEM-1-*O*-gluc-2′-benzyl alcohol	
Structure	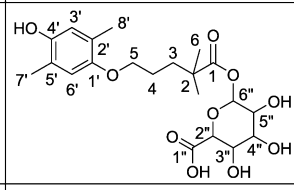		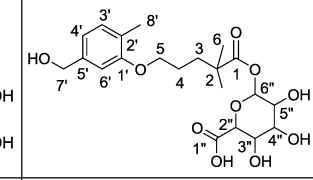		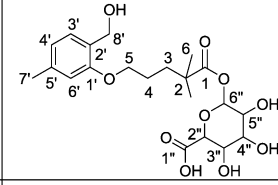	
λ_{max}, nm	290		276		276	
MS, *m*/*z*[a]	441		441		441	
MS^2, *m*/*z*	265, 175, 137, 113		265, 175, 137, 113		265, 175, 137, 135, 113	
NMR[b]	^{1}H and ^{13}C δ (ppm) and Multiplicity					
	^{1}H NMR	^{13}C NMR	^{1}H NMR	^{13}C NMR	^{1}H NMR	^{13}C NMR
5	3.91 (m)	N.A.	3.92 (m)	75.7	3.91 (m)	N.A.
1′	-	149.5	-	157.2	-	N.A.
2′	-	121.6	-	124.4	-	128.1
3′	6.51 (br s)	117.2	7.40 (d, *J* = 7.5 Hz)	130.3	7.22 (d, *J* = 8.3 Hz)	N.A.
4′	-	149.1	6.75 (dd, *J* = 7.5, 2.0 Hz)	118.5	6.72 (dd, *J* = 2.0, 8.3 Hz)	121.0
5′	-	124.1	-	142.0	-	137.2
6′	6.58 (br s)	116.1	6.87 (d, *J* = 2.0 Hz)	110.2	6.73 (s)	112.6
7′	2.03 (br s)	16.51	4.43 (br s)	63.7	2.27 (s)	N.A.
8′	2.01 (br s)	15.98	2.12 (s)	16.6	4.46 (br s)	N.A.

[a] Mass spectra were acquired following ESI−. [b] Chemical shift assignments were made from 1D ^{1}H, 1D TOCSY, 1D NOESY, and 2D gHMBCAD NMR spectra. Data are shown only for the 2′,5′-dimethylphenoxy portion of GEM-1-*O*-gluc because this is the region that is modified. Chemical shift values are expressed in ppm relative to the residual solvent peak (2.50 ppm). Because of low signal for metabolites M1 and M3, not all ^{1}H and ^{13}C chemical shifts could be confirmed and are not assigned (N.A.). The dash (—) indicates that there is no proton on the corresponding carbon.

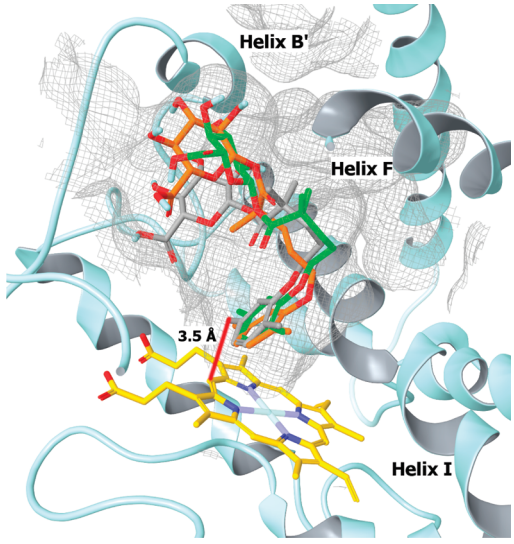

Figure 8. Computational model of P450 2C8 with GEM-1-*O*-gluc docked in the active site. Representative docking orientations of GEM-1-*O*-gluc are shown in computational models from solved X-ray crystal structures of P450 2C8 (orange structure), P450 2C8 with retinoic acid (gray structure), or P450 2C8 with montelukast (green structure). For simplicity, only portions of the secondary structure are shown for the structure of substrate-free P450 2C8 (cyan ribbon). Oxygen atoms are colored red, nitrogen atoms are colored blue, and the heme structure is colored yellow. The solvent-accessible surface of the active site cavity is designated by the gray mesh.

oxidation, could lead to a reactive quinone metabolite (*10*). The resultant quinone (or quinone-methide) metabolite could react with a nucleophilic residue within the active site of P450 2C8 and terminate catalytic activity, as exemplified by the covalent binding of raloxifene to a P450 3A4 active site cysteine residue (*23*). In the current work, chromatographic and mass analysis of intact recombinant P450 2C8, following a reaction with GEM-1-*O*-gluc and NAPDH, did not reveal such a drug adduct to the apoprotein but instead provided evidence for GEM-1-*O*-gluc addition to the heme prosthetic group of the P450.

When the reaction mixture containing P450 2C8 and GEM-1-*O*-gluc was separated chromatographically, an NADPH-dependent peak was apparent, which eluted slightly after native heme and, like native heme, absorbed in the 400 nm region of the electronic spectrum. The corresponding molecular ion, at *m*/*z* 1040.7, was consistent with a mass equal to 1 equiv of GEM-1-*O*-gluc, plus heme, minus two hydrogen atoms. The loss of two hydrogen atoms upon covalent binding to the heme indicated that the molecule of GEM-1-*O*-gluc was not linked to a nitrogen atom of the heme pyrrole groups, as observed with heme adducts formed following bioactivation of acetylene and hydrazine functional groups. Only a single hydrogen atom is lost, from the substrate, when the iron−nitrogen coordinate bond is broken in the formation of an *N*-alkyl heme adduct, whereas two hydrogen atoms are lost, one from the substrate and one from the heme, when a substrate is covalently bound to a carbon atom on the heme periphery. This point is exemplified by the loss of a single hydrogen atom with the *N*-linked 17α-ethynylestradiol heme adduct formed with P450 3A5 (*24*), as compared to the loss of two hydrogen atoms with γ-meso linked 3-phenylethyl adduct formed with P450 2B4 (*25*).

Computational models of P450 2C8, built from solved X-ray crystal structures, were utilized to evaluate further the potential site of covalent attachment of GEM-1-*O*-gluc to the heme. Mapping of the solvent-accessible surface area in the active site demonstrated that only portions the C and D pyrrole groups of

heme were exposed, including the γ-meso carbon and pyrrole nitrogens, but excluded the methyl groups on the periphery (*26, 27*) (Figure 8). When GEM-1-*O*-gluc was docked into the P450 2C8 computational model, the 2′,5′-dimethylphenoxy group consistently was oriented directly over the γ-meso carbon. The energy-minimized conformations of GEM-1-*O*-gluc did not approach any other atom on the heme periphery. Although the computational modeling indicated that the γ-meso carbon of heme was likely the site of covalent attachment, NMR analysis of the purified heme adduct will be required to confirm that GEM-1-*O*-gluc is not bound to an alternate meso-position or to a methyl or a vinyl substituent of heme. Interestingly, heme adducts at the γ-meso carbon have been characterized previously in the reactions of 3-phenylpropionaldehyde with either P450 2B4 or $P450_{BM3}$ F87G, but substrate addition to other carbon positions on the periphery of P450 heme has not been reported in the literature, to date (*25, 28*). The P450 2B4 3-phenylethyl heme adduct, whose structure has been confirmed by NMR analysis, exhibited a similar λ_{max} value (408 nm) in the electronic absorption spectrum as did the P450 2C8 GEM-1-*O*-gluc heme adduct (407 nm), providing additional support for alkylation at a meso-position.

Fragment ions of the GEM-1-*O*-gluc-heme adduct in the MS^2 and MS^3 spectra provided evidence for a covalent linkage between the 2′,5′-dimethylphenoxy group of GEM-1-*O*-gluc and heme but did not distinguish between a methyl vs aromatic linkage on GEM-1-*O*-gluc. Therefore, an analogue of GEM-1-*O*-gluc, in which both benzylic positions were fully deuterated (GEM-d_6-1-*O*-gluc), was utilized to further characterize the covalently modified heme and the mechanism of its formation. Mass analysis of the resulting heme adduct revealed that a single deuterium atom had been eliminated during the reaction, implicating one of the two benzylic carbons of GEM-1-*O*-gluc as the site of covalent bond formation. In support of this finding, computational docking of GEM-1-*O*-gluc in solved X-ray crystal structures of P450 2C8 revealed that both benzylic carbons could be directed within 3−4 Å of the γ-meso position on the heme (Figure 8). Because of the rotameric flexibility of the alkyl chain of GEM-1-*O*-gluc, there was no indication that either the 2′-methyl or the 5′-methyl group would have a favored orientation. Overall, data were in agreement with a GEM-1-*O*-gluc-heme adduct chemical structure in which a benzylic carbon on the 2′,5′-dimethylphenoxy group of GEM-1-*O*-gluc was covalently bound to the γ-meso carbon of the heme (Scheme 1).

Formation of all experimentally characterized hemoprotein heme-substrate adducts, whether bound to the iron atom, pyrrole nitrogens, pyrrole carbons, vinyl groups, or meso-carbons, involves generation of a radical species via single electron oxidation, which subsequently reacts with the heme group of the enzyme (*29*). In the catalytic cycle of P450 enzymes, transient substrate radicals are routinely generated by oxidation with its iron-oxo species of heme ($Por^{+\bullet}Fe^{IV}$=O) (*30*). The substrate radical is typically short-lived, as oxygen rebound, or second electron transfer, quickly follows to complete the two electron oxidation of the substrate (*30*). High intrinsic kinetic deuterium isotope effects, in addition to extensive scrambling of regiochemistry and stereochemistry of substrates in P450-catalyzed carbon hydroxylation reactions, have provided evidence for hydrogen atom abstraction and, therefore, the substrate radical intermediate (*30*). In the mechanism of P450 2C8 inactivation by GEM-1-*O*-gluc, the benzyl radical, formed by oxidation of either the 2′- or the 5′-methyl on the 2′,5′-dimethylphenoxy group, was likely the species that reacted with the γ-meso position of heme prosthetic group. The reaction with

Scheme 1. Proposed Mechanism for the Covalent Attachment of GEM-1-*O*-gluc to the Heme of P450 2C8[a]

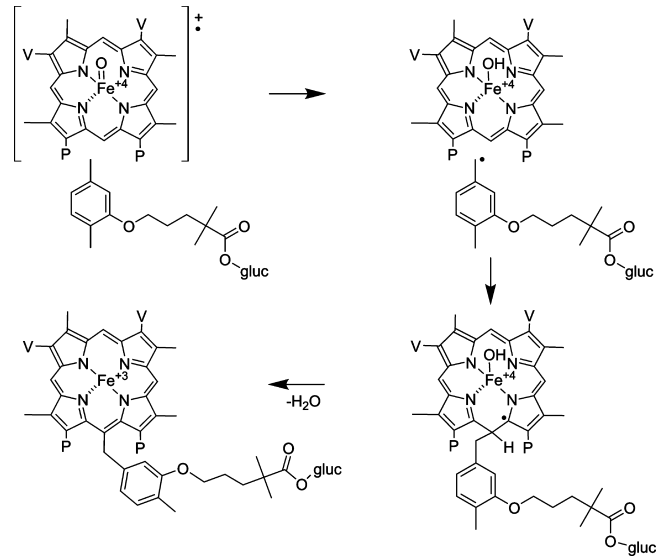

[a] Propionate and vinyl groups of heme are designated by "P" and "V", respectively, and the glucuronide group of GEM-1-*O*-gluc is abbreviated "gluc". The benzylic carbon at the 2′-position (as shown) or the 5′-position on the 2′,5′-dimethylphenoxy group of GEM-1-*O*-gluc, or both, may be involved in the mechanism of covalent attachment of GEM-1-*O*-gluc to heme. The site of covalent modification on the heme has not been confirmed experimentally, but computational modeling studies indicated that GEM-1-*O*-gluc had access to the γ-meso carbon.

the heme could be modeled after the mechanisms that have been proposed for the covalent binding of alkyl, aryl, azidyl, acetyl, cyanyl, and chloride radicals, to the δ-meso position of horseradish peroxidase heme (*29, 31*) or alkyl radicals to the γ-meso position of myoglobin heme (*32*) and P450 2B4 heme (*25*). In these mechanisms, substrate radical addition to the meso-position of compound II, or equivalent oxidized heme species ($PorFe^{IV}$−OH), is followed by electron redistribution to the iron atom from the periphery. Loss of the meso-proton finally produces the meso-alkylated heme. The analogous mechanism for addition of the GEM-1-*O*-gluc radical to the γ-meso carbon is shown in Scheme 1.

The role of the benzyl radical in the mechanism of P450 2C8 inactivation was supported by the observed deuterium isotope effects in the time-dependent inactivation experiments. When GEM-d_6-1-*O*-gluc was incubated with P450 2C8, the k_{inact} decreased 2.2-fold, as compared to the rate of inactivation by GEM-1-*O*-gluc, while the K_I was identical. This result indicated that hydrogen atom abstraction from a benzylic position on GEM-1-*O*-gluc and, therefore, formation of a benzyl radical, was the rate-determining step in the inactivation of P450 2C8. The accompanying 1.7-fold decrease in the amount of GEM-1-*O*-gluc-heme adduct formed when GEM-d_6-1-*O*-gluc was used as a substrate, vs GEM-1-*O*-gluc, provided a correlation between the inactivation of P450 2C8 and the time-dependent inactivation, two events that were each dependent on hydrogen atom abstraction from a benzylic carbon. Intriguingly, the magnitude of the deuterium isotope effect in this system was similar to the 2-fold decrease in the rate of inactivation of P450 1A2 measured when the imidazo-methyl group of furafylline was fully deuterated (*33*). Similar to the bioactivation mechanism of GEM-1-*O*-gluc, the carbon−hydrogen bond cleavage on the heteroaromatic methyl group of furafylline was a critical event leading to inhibition of P450 1A2, although the fate of the resulting radical differed. In the case of furafylline, the methyl

radical partially evaded recapture by the iron-bound hydroxyl radical, as did the GEM-1-*O*-gluc benzyl radical, but instead of adding to the heme, the furafylline radical likely led to an electrophilic imidazomethide intermediate that reacted with active site residues (*34*).

The benzyl radical of GEM-1-*O*-gluc is not especially reactive, as compared to radicals involved in formation of meso-carbon adducts with the heme of horseradish peroxidase (*29, 31*). The bond dissociation energy, which is a good indicator of the radical energy (*31*), is estimated to be approximately 86.2 kcal/mol for a benzyl radical with a *p*-methyl group (*35*), although the value would be affected slightly depending on the relative location of the alkyloxy group on the aromatic group of GEM-1-*O*-gluc (*m*-alkyloxy group relative to the benzyl radical would decrease the energy, but the effects of a *o*-alkyloxy group are less predictable). This estimated value is near the lower limit (88 ± 1 kcal/mol) that Worjciechowski and Ortiz de Montellano have identified as the minimal energy needed to react with a meso-carbon on compound II of horseradish peroxidase (*31*). To date, there is no available correlation of radical energies with relative reactivity toward the meso-position of the compound II-equivalent of P450 heme. However, the relative stability of the benzyl radical does suggest that there were other factors facilitating addition of the GEM-1-*O*-gluc radical to the meso-carbon vs oxygen rebound to form hydroxylated metabolites. Computational modeling of GEM-1-*O*-gluc in the active site of P450 2C8 demonstrated that the benzylic carbons of GEM-1-*O*-gluc were consistently oriented either upward and away from the heme iron or toward the γ-meso position of heme (Figure 8). The fact that the methyl groups of GEM-1-*O*-gluc, in energy-minimized conformations, were never directed toward the heme center signified that protein matrix constraints could have influenced the fate of the benzyl radical. Constraints imposed by active site residues may have helped to reposition an oxidized methyl group near the γ-meso carbon on heme, within the lifetime of the relatively stable benzyl radical and, therefore, could have increased the probability of heme adduct formation vs oxygen rebound.

The efficiency of a mechanism-based inhibitor is defined by its partition ratio, which is the ratio of all metabolic events pertaining to the inhibitor, divided by the number of enzyme inactivating events. The sum of metabolic events includes metabolic events lying along the reaction coordinate leading to inactivation, which includes noninactivating branching to stable metabolites, as well as metabolic events at distal sites on the substrate (*33*). The measured partition ratio for the inactivation of P450 2C8 by GEM-1-*O*-gluc was 53, a relatively high value as compared to the partition ratios that have been calculated for numerous mechanism-based inhibitors of P450 3A4 (*36*). The noninactivating metabolic events in the reaction of P450 2C8 with GEM-1-*O*-gluc could be explained by the formation of 4′-hydroxy-GEM-1-*O*-gluc (M1), GEM-1-*O*-gluc-5′-benzyl alcohol (M2), and GEM-1-*O*-gluc-2′-benzyl alcohol (M3). Generation of M2 and M3 would have involved formation of benzyl radical intermediates prior to oxygen rebound; therefore, one or both of these metabolites lie along the reaction coordinate leading to GEM-1-*O*-gluc-heme adduct formation and inactivation. Involvement of a common intermediate was supported by the similar concentrations of benzyl alcohol metabolites found in reactions with GEM-d_6-1-*O*-gluc, as in reactions with the unlabeled substrate, following complete inactivation of P450 2C8.

Because of the "commitment to catalysis" of P450 following substrate binding, intrinsic kinetic deuterium isotope effects are masked, unless there is a branched reaction pathway from the substrate-bound active perferryl oxene species ($Por^{+\bullet}Fe^{IV}=O$) to an alternate product, or if the perferryl oxene is reduced to produce free substrate, free enzyme, and water (*37*). In the reaction of P450 2C8 and GEM-d_6-1-*O*-gluc, unmasking of the intrinsic deuterium isotope on k_{inact}, and the resulting increase in the calculated partition ratio, could be explained by metabolic switching away from benzylic oxidation (M2, M3, heme adduct) to 4′-hydroxy-GEM-1-*O*-gluc formation (M1). Similar metabolic switching has been characterized previously in the metabolism of toluene-d_3 by liver microsomes from phenobarbital-induced rats (*38*). In this system, the observed deuterium isotope effect for benzyl alcohol formation [$^{D}V = 1.92$ and $^{D}(V/K) = 3.53$] could be accounted for by the increase in cresol formation. Unfortunately, a complete stoichiometric analysis, which could account for the 1.8-fold change in partition ratio, could not be performed with GEM-1-*O*-gluc metabolites due to the lack of standards and the fact that the extinction coefficients assuredly were altered with aromatic ring oxidation.

Formation of the 4′-hydroxy-GEM-1-*O*-gluc metabolite (M1) in the reaction of GEM-1-*O*-gluc with P450 2C8 presented the possibility that a reactive quinone intermediate could have contributed to the mechanism-based inactivation of the P450, as originally proposed by Ogilvie et al. (*10*). Metabolite M1 was especially suspect because it was unstable following extraction, and a degradation product from this appeared to be loss of the 4′-hydroxy-2′,5′-dimethylphenoxy group. It was possible that chemical oxidation of 4′-hydroxy-GEM-1-*O*-gluc led to the cleavage of the carbon−oxygen ether bond, similar to the P450 3A4- and P450 2C8-mediated oxidation of troglitazone to a quinone type metabolite (*39*). If this reaction had occurred during the incubation, mediated either chemically or enzymatically, the quinone metabolite could have reacted with nucleophilic amino acid residues within the active site of P450 2C8 and inactivated the enzyme. Despite these findings, there was no evidence for an apoprotein adduct in the mass spectrum of the intact protein. In addition, incubations with P450 2C8 and GEM-d_6-1-*O*-gluc demonstrated a 2.2-fold decrease in k_{inact} and an increase in the partition ratio, despite the 6-fold increase in the production of metabolite M1. On the basis of these facts, it was apparent that even if the quinone intermediate was formed during oxidation of GEM-1-*O*-gluc, it was not the major metabolite intermediate responsible for the observed inactivation of P450 2C8.

Collectively, the data indicated that P450 2C8 oxidized GEM-1-*O*-gluc to a benzyl radical intermediate that partitioned between oxygen rebound and addition to the γ-meso carbon of heme. The deviation from the typical P450 reaction cycle may have been due to protein control over the repositioning of the oxidized 2′,5′-dimethylphenoxy group, within the lifetime of the benzyl radical, away from the iron center and toward the heme periphery. Formation of the GEM-1-*O*-gluc-heme adduct most assuredly would block additional substrates from accessing the catalytic heme center of P450 2C8 and result in the observed mechanism-based inhibition.

Acknowledgment. We thank Rheem Totah at the University of Washington for the stock of recombinant P450 2C8 used for preliminary experiments and the *E. coli* DH5α cells, transformed with the P450 2C8-containing pCW expression vector. We also thank Michael L. Schrag for insightful discussions.

References

(1) Backman, J. T., Kyrklund, C., Neuvonen, M., and Neuvonen, P. J. (2002) Gemfibrozil greatly increases plasma concentrations of cerivastatin. *Clin. Pharmacol. Ther. 72*, 685–691.

(2) Niemi, M., Backman, J. T., Neuvonen, M., and Neuvonen, P. J. (2003) Effects of gemfibrozil, itraconazole, and their combination on the pharmacokinetics and pharmacodynamics of repaglinide: Potentially hazardous interaction between gemfibrozil and repaglinide. *Diabetologia 46*, 347–351.

(3) Niemi, M., Backman, J. T., Granfors, M., Laitila, J., Neuvonen, M., and Neuvonen, P. J. (2003) Gemfibrozil considerably increases the plasma concentrations of rosiglitazone. *Diabetologia 46*, 1319–1323.

(4) Jaakkola, T., Backman, J. T., Neuvonen, M., and Neuvonen, P. J. (2005) Effects of gemfibrozil, itraconazole, and their combination on the pharmacokinetics of pioglitazone. *Clin. Pharmacol. Ther. 77*, 404–414.

(5) Wen, X., Wang, J. S., Backman, J. T., Kivisto, K. T., and Neuvonen, P. J. (2001) Gemfibrozil is a potent inhibitor of human cytochrome P450 2C9. *Drug Metab. Dispos. 29*, 1359–1361.

(6) Wang, J. S., Neuvonen, M., Wen, X., Backman, J. T., and Neuvonen, P. J. (2002) Gemfibrozil inhibits CYP2C8-mediated cerivastatin metabolism in human liver microsomes. *Drug Metab. Dispos. 30*, 1352–1356.

(7) Lilja, J. J., Backman, J. T., and Neuvonen, P. J. (2005) Effect of gemfibrozil on the pharmacokinetics and pharmacodynamics of racemic warfarin in healthy subjects. *Br. J. Clin. Pharmacol. 59*, 433–439.

(8) Shitara, Y., Hirano, M., Sato, H., and Sugiyama, Y. (2004) Gemfibrozil and its glucuronide inhibit the organic anion transporting polypeptide 2 (OATP2/OATP1B1:SLC21A6)-mediated hepatic uptake and CYP2C8-mediated metabolism of cerivastatin: analysis of the mechanism of the clinically relevant drug-drug interaction between cerivastatin and gemfibrozil. *J. Pharmacol. Exp. Ther. 311*, 228–236.

(9) Mano, Y., Usui, T., and Kamimura, H. (2007) The UDP-glucuronosyltransferase 2B7 isozyme is responsible for gemfibrozil glucuronidation in the human liver. *Drug Metab. Dispos. 35*, 2040–2044.

(10) Ogilvie, B. W., Zhang, D., Li, W., Rodrigues, A. D., Gipson, A. E., Holsapple, J., Toren, P., and Parkinson, A. (2006) Glucuronidation converts gemfibrozil to a potent, metabolism-dependent inhibitor of CYP2C8: Implications for drug-drug interactions. *Drug Metab. Dispos. 34*, 191–197.

(11) Sallustio, B. C., and Foster, D. J. (1995) Reactivity of gemfibrozil 1-*O*-beta-acyl glucuronide. Pharmacokinetics of covalently bound gemfibrozil-protein adducts in rats. *Drug Metab. Dispos. 23*, 892–899.

(12) Hinton, L. K., Galetin, A., and Houston, J. B. (2008) Multiple inhibition mechanisms and prediction of drug-drug interactions: Status of metabolism and transporter models as exemplified by gemfibrozil-drug interactions. *Pharm. Res. 25*, 1063–1074.

(13) Prueksaritanont, T., Zhao, J. J., Ma, B., Roadcap, B. A., Tang, C., Qiu, Y., Liu, L., Lin, J. H., Pearson, P. G., and Baillie, T. A. (2002) Mechanistic studies on metabolic interactions between gemfibrozil and statins. *J. Pharmacol. Exp. Ther. 301*, 1042–1051.

(14) Tornio, A., Niemi, M., Neuvonen, M., Laitila, J., Kalliokoski, A., Neuvonen, P. J., and Backman, J. T. (2008) The effect of gemfibrozil on repaglinide pharmacokinetics persists for at least 12 h after the dose: Evidence for mechanism-based inhibition of CYP2C8 in vivo. *Clin. Pharmacol. Ther. 84*, 403–411.

(15) Fontana, E., Dansette, P. M., and Poli, S. M. (2005) Cytochrome P450 enzymes mechanism based inhibitors: Common sub-structures and reactivity. *Curr. Drug Metab. 6*, 413–454.

(16) Gillam, E. M., Baba, T., Kim, B. R., Ohmori, S., and Guengerich, F. P. (1993) Expression of modified human cytochrome P450 3A4 in *Escherichia coli* and purification and reconstitution of the enzyme. *Arch. Biochem. Biophys. 305*, 123–131.

(17) Holmans, P. L., Shet, M. S., Martin-Wixtrom, C. A., Fisher, C. W., and Estabrook, R. W. (1994) The high-level expression in *Escherichia coli* of the membrane-bound form of human and rat cytochrome b5 and studies on their mechanism of function. *Arch. Biochem. Biophys. 312*, 554–565.

(18) Porter, T. D., Wilson, T. E., and Kasper, C. B. (1987) Expression of a functional 78,000 Da mammalian flavoprotein, NADPH-cytochrome P-450 oxidoreductase, in *Escherichia coli*. *Arch. Biochem. Biophys. 254*, 353–367.

(19) Sajiki, H., Ito, N., Esaki, H., Maesawa, T., Maegawa, T., and Hirota, K. (2005) Aromatic ring favorable and efficient H-D exchange reaction catalyzed by Pt/C. *Tetrahedron Lett. 46*, 6995–6998.

(20) Walsky, R. L., and Obach, R. S. (2004) Validated assays for human cytochrome P450 activities. *Drug Metab. Dispos. 32*, 647–660.

(21) Silverman, R. B. (1996) Mechanism-based enzyme inactivators. In *Contemporary Enzyme Kinetics and Mechanism* (Purich, D., Ed.) pp 291−335, Academic Press, San Diego, CA.

(22) Thomas, B. F., Burgess, J. P., Coleman, D. P., Scheffler, N. M., Jeffcoat, A. R., and Dix, K. J. (1999) Isolation and identification of novel metabolites of gemfibrozil in rat urine. *Drug Metab. Dispos. 27*, 147–157.

(23) Baer, B. R., Wienkers, L. C., and Rock, D. A. (2007) Time-dependent inactivation of P450 3A4 by raloxifene: Identification of Cys239 as the site of apoprotein alkylation. *Chem. Res. Toxicol. 20*, 954–964.

(24) Lin, H. L., and Hollenberg, P. F. (2007) The inactivation of cytochrome P450 3A5 by 17alpha-ethynylestradiol is cytochrome b5-dependent: metabolic activation of the ethynyl moiety leads to the formation of glutathione conjugates, a heme adduct, and covalent binding to the apoprotein. *J. Pharmacol. Exp. Ther. 321*, 276–287.

(25) Kuo, C. L., Raner, G. M., Vaz, A. D., and Coon, M. J. (1999) Discrete species of activated oxygen yield different cytochrome P450 heme adducts from aldehydes. *Biochemistry 38*, 10511–10518.

(26) Schoch, G. A., Yano, J. K., Wester, M. R., Griffin, K. J., Stout, C. D., and Johnson, E. F. (2004) Structure of human microsomal cytochrome P450 2C8. Evidence for a peripheral fatty acid binding site. *J. Biol. Chem. 279*, 9497–9503.

(27) Schoch, G. A., Yano, J. K., Sansen, S., Dansette, P. M., Stout, C. D., and Johnson, E. F. (2008) Determinants of cytochrome P450 2C8 substrate binding: structures of complexes with montelukast, troglitazone, felodipine, and 9-cis-retinoic acid. *J. Biol. Chem. 283*, 17227–17237.

(28) Raner, G. M., Hatchell, A. J., Morton, P. E., Ballou, D. P., and Coon, M. J. (2000) Stopped-flow spectrophotometric analysis of intermediates in the peroxo-dependent inactivation of cytochrome P450 by aldehydes. *J. Inorg. Biochem. 81*, 153–160.

(29) Ortiz de Montellano, P. R. (1990) Free radical modification of prosthetic heme groups. *Pharmacol. Ther. 48*, 95–120.

(30) Guengerich, F. P. (2001) Common and uncommon cytochrome P450 reactions related to metabolism and chemical toxicity. *Chem. Res. Toxicol. 14*, 611–650.

(31) Wojciechowski, G., and de Montellano, P. R. (2007) Radical energies and the regiochemistry of addition to heme groups. Methylperoxy and nitrite radical additions to the heme of horseradish peroxidase. *J. Am. Chem. Soc. 129*, 1663–1672.

(32) Choe, Y. S., and Ortiz de Montellano, P. R. (1991) Differential additions to the myoglobin prosthetic heme group. Oxidative gamma-meso substitution by alkylhydrazines. *J. Biol. Chem. 266*, 8523–8530.

(33) Kunze, K. L., and Trager, W. F. (1993) Isoform-selective mechanism-based inhibition of human cytochrome P450 1A2 by furafylline. *Chem. Res. Toxicol. 6*, 649–656.

(34) Racha, J. K., Rettie, A. E., and Kunze, K. L. (1998) Mechanism-based inactivation of human cytochrome P450 1A2 by furafylline: Detection of a 1:1 adduct to protein and evidence for the formation of a novel imidazomethide intermediate. *Biochemistry 37*, 7407–7419.

(35) Khursan, S. L., Mikhailov, D. A., Yanborisov, V. M., and Borisov, D. I. (1997) AM1 calculations of bond dissociation energies. Allylic and benzylic C-H bonds. *React. Kinet. Catal. Lett. 61*, 91–95.

(36) Zhou, S., Yung Chan, S., Cher Goh, B., Chan, E., Duan, W., Huang, M., and McLeod, H. L. (2005) Mechanism-based inhibition of cytochrome P450 3A4 by therapeutic drugs. *Clin. Pharmacokinet. 44*, 279–304.

(37) Nelson, S. D., and Trager, W. F. (2003) The use of deuterium isotope effects to probe the active site properties, mechanism of cytochrome P450-catalyzed reactions, and mechanisms of metabolically dependent toxicity. *Drug Metab. Dispos. 31*, 1481–1498.

(38) Ling, K. H., and Hanzlik, R. P. (1989) Deuterium isotope effects on toluene metabolism. Product release as a rate-limiting step in cytochrome P-450 catalysis. *Biochem. Biophys. Res. Commun. 160*, 844–849.

(39) Yamazaki, H., Shibata, A., Suzuki, M., Nakajima, M., Shimada, N., Guengerich, F. P., and Yokoi, T. (1999) Oxidation of troglitazone to a quinone-type metabolite catalyzed by cytochrome P-450 2C8 and P-450 3A4 in human liver microsomes. *Drug Metab. Dispos. 27*, 1260–1266.

TX900105N